RESEARCH ARTICLE | APRIL 13 2026

# An accurate and automated approach for the quantification of single-cell adhesion dynamics from microscopy images

Marilisa Cortesi ; Jingjing Li ; Dongli Liu ; Tianruo Guo; Socrates Dokos ; Kristina Warton; Caroline E. Ford



*Biophysics Rev.* 7, 021401 (2026)
https://doi.org/10.1063/5.0293339

# An accurate and automated approach for the quantification of single-cell adhesion dynamics from microscopy images

Cite as: Biophysics Rev. **7**, 021401 (2026); doi: 10.1063/5.0293339
Submitted: 12 August 2025 · Accepted: 24 March 2026 ·
Published Online: 13 April 2026



Marilisa Cortesi,[1,a)] Jingjing Li,[2] Dongli Liu,[3] Tianruo Guo,[2] Socrates Dokos,[2] Kristina Warton,[3] and Caroline E. Ford[3,b)]

## AFFILIATIONS

[1]Laboratory of Cellular and Molecular Engineering, Department of Electrical Electronic and Information Engineering "G. Marconi," Alma Mater Studiorum—University of Bologna, Cesena, Italy
[2]Gynaecological Cancer Research Group, School of Clinical Medicine, Faculty of Medicine and Health, University of New South Wales, Kensington, New South Wales, Australia
[3]Graduate School of Biomedical Engineering, University of New South Wales, Sydney, New South Wales, Australia

[a)]**Author to whom correspondence should be addressed:** marilisa.cortesi2@unibo.it
[b)]**Electronic mail:** caroline.ford@unsw.edu.au

## ABSTRACT

Cell adhesion is a key property of cancer cells, as it relates to their potential for dissemination and metastasis. The *in vitro* assays used to measure it and, however, are characterized by several drawbacks, including low temporal resolution and limited procedural standardization, which reduce their usefulness and accuracy. In this work, we propose an alternative analytical approach, based on live-cell imaging, which enables the study of cell adhesion dynamics at the single-cell level. The increased resolution afforded by this method was instrumental for the identification of cell division prior to attachment and the co-existence of markedly different proliferation rates across the culture, previously unidentified patterns of behavior in the adhesion process. Finally, we generalize our method by substituting the segmentation algorithm and showing that this approach can be integrated within routine laboratory analytical procedures and does not require high-performance microscopy and imaging setups. Our new analytical approach improves the *in vitro* quantification of cell adhesion, enabling the study of this process with high temporal resolution and increased level of detail. The extension of the analysis to the single-cell level, additionally, uncovered the role of population variability and proliferation in this process. The simple and cost-effective procedure here described enables the accurate characterization of cell adhesion. In addition to improving our understanding of adhesion dynamics, its results could support the development of treatments targeting the ability of cancer cells to adhere to surrounding tissues by allowing detailed quantification of cell adhesion metrics.





## I. BACKGROUND

The ability of cancer cells to adhere to a given substrate is a key property, which can provide insight into their metastatic potential as swift and robust adhesion to healthy tissue is a key step toward its colonization. The *in vitro* study of this phenomenon largely consists of (i) seeding a known number of cells on the substrate of interest, (ii) waiting a set amount of time, (iii) washing away the non-attached cells, and (iv) quantifying the density of the adherent population, generally through an absorbance measurement.[1,2] While procedurally simple and largely accessible, this assay is characterized by many drawbacks. These include binary classification as attached/detached, rather than identification of the different adhesion phases, and restriction of the analysis to population level, which eliminates intercellular variability, a fundamental element of cancer progression and metastasis initiation.[3] The results are also dependent on the intensity of the washing step, which is difficult to standardize and could potentially vary between samples and operators. While alternative methods are available,[4] and some of them enable the evaluation of single-cell adhesion strength,[5] they generally require specific instrumentation, and the experimental conditions tend to be quite far from *in vivo*-like culturing setups.

Live-cell imaging analysis offers a potential solution. Indeed, different adhesion stages result in morphological changes in the cells,[6] which can be identified with an appropriate segmentation and classification routine. An advantage of these setups is that they maintain cells in standard culturing conditions, thus minimizing the effect of the measurement on the biological process itself.[7–9]

In this study, we evaluated the feasibility of this approach by using an IncuCyte S3 Live Cell Analysis system to acquire images of two different ovarian cancer (OC) cell lines (PEO1 and PEO4) as they adhered to the bottom of a multi-well plate. OC is a particularly interesting application as it disseminates predominantly through the transcoelomic route, a process by which cancer cells spread across the peritoneal space rather than by infiltrating the circulatory system.[10,11] The ability to effectively and quickly adhere to the substrate is thus fundamental for disease progression and metastasis in OC. Metastasis formation is also common, with more than 75% of patients presenting at diagnosis with metastatic disease,[12] and bears a strong association with poor outcome and the development of drug resistance.[13,14] The selection of PEO1 and PEO4 cells is also relevant. Both are derived from the same patient with high-grade serous OC but represent different stages of disease progression: first recurrence (PEO1) and the development of treatment resistance (PEO4).[15] These features make them highly comparable while allowing for a range of behaviors to be explored.

Our results show that cell adhesion is a highly heterogeneous and dynamic process and provide a novel approach to quantify it at high resolution and in an operator independent, highly automated manner.

## II. RESULTS

Adhesion was monitored in PEO1 and PEO4 cells by placing cultures of these cells into an IncuCyte S3 Live Cell Analysis system immediately after seeding. Three different cell densities (1000, 2000, and 4000 cells/well) were used to showcase the versatility of this method and its performance across the range of seeding densities generally used for *in vitro* assays. Images of the same area of the culture were acquired for 20 h with a temporal resolution of 30 min. Analysis of these images (further details in Sec. V) enabled the determination of each cell's adhesion status.

### A. Adhesion at the population level is dynamic and cell line-dependent

The same qualitative behavior was observed at the population level for all conditions: the fraction of detached cells decreased as that of partially attached, and fully attached cells increased (Fig. 1). However, cell line-specific dynamics were also observed. PEO1 cells adhered more quickly, with the population of detached cells dropping below 20% before the end of the experiment, and the rest of the population uniformly split between partially and fully attached. PEO4 cells, on the other hand, remained mostly in the intermediate, partially attached state, with only about 20% of the cells attaining complete adhesion after 20 h. This is also confirmed by the representative images shown in Figs. 1(d) and 1(h).

Changing the initial cell density (1000, 2000, or 4000 cells/well) affected the behavior of PEO1 cells, with a reduction in adhesion speed proportional to the population size. Indeed, the time point at which the fully attached population becomes more prevalent than the detached population is 7 h for the 1000 cells/well, 10 h for 2000 cells/well, and 13 h for 4000 cells/well. This effect is not present for PEO4 cells, where the difference in prevalence between the different classes is largely conserved when changing the seeding density.

This is coherent with PEO4 cells being derived from a more advanced, aggressive disease stage. Adhesion assays conducted using

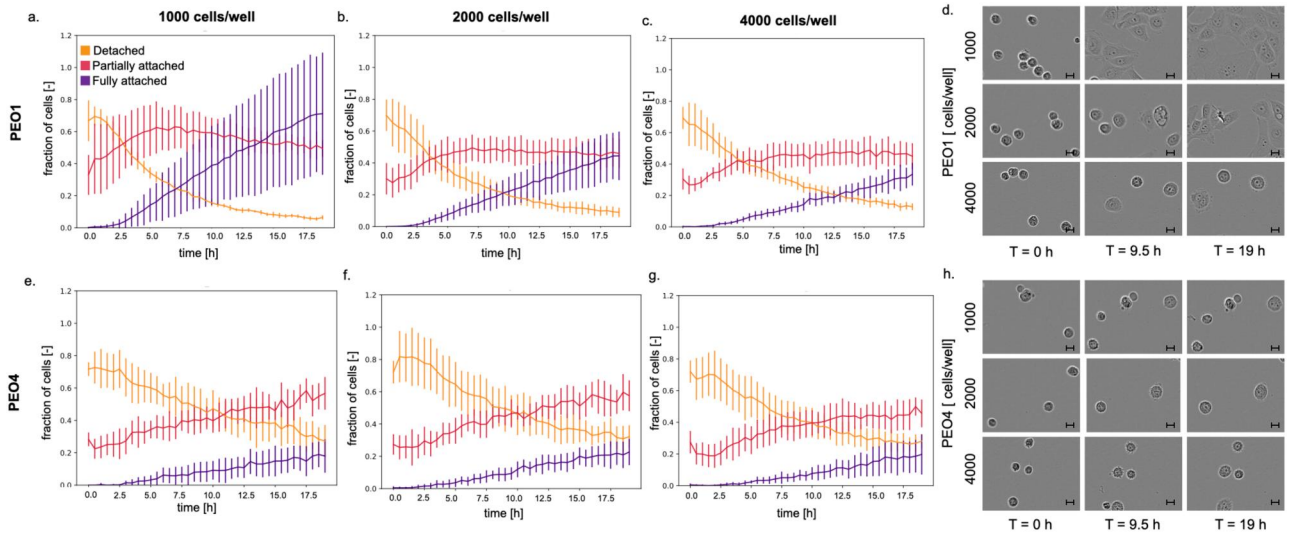


**FIG. 1.** Global adhesion analysis showing the prevalence of each adhesion class over time. Average and standard deviation of the fraction of cells for each adhesion status (orange—detached; red—partially attached; and purple—fully attached) as measured for PEO1 cells with an initial cell density of (a) 1000 cells/well, (b) 2000 cells/well, and (c) 4000 cells/well (three wells and three images/well). (e)–(g) are the same as (a)–(c) but for PEO4 cells. In all cases, the fraction of cells was normalized with respect to the initial population size. Panels (d) and (h) show three representative images for each condition, acquired at the beginning, middle, and end of the experiment. The scale bars correspond to 10 $\mu$m.

**TABLE I.** Summary of the different adhesion dynamics, their definition, and associated number and color.

| | Adhesion dynamic | Definition | Color |
|---|---|---|---|
| 1 | Short | Track with less than four time points (equivalent length of 2 h) | |
| 2 | Flat detached | Negligible variation, cell classified as detached | |
| 3 | Flat partially attached | Negligible variation, cell classified as partially attached | |
| 4 | Monotonal detaching | Monotonal track leading to cell detachment | |
| 5 | Monotonal partially attached | Monotonal track with partial attachment of the cell | |
| 6 | Monotonal fully attached | Monotonal track with full attachment of the cell | |
| 7 | Non-monotonal partially attached | Non-monotonal track with partial attachment of the cell | |
| 8 | Non-monotonal fully attached | Non-monotonal track with one full attachment of the cell | |
| 9 | Non-monotonal fully attached More than once | Non-monotonal track with Multiple full attachments of the cell | |

the standard approach by Ritch *et al.* yielded comparable results: PEO1 cells adhered more, with a faster dynamic when compared with PEO4 cells.[16] The time courses presented here, however, are characterized by a higher temporal resolution (30 min instead of a few hours) and enable the identification of the different adhesion phases.

## B. Distinct adhesion dynamics are identified by single-cell level adhesion analysis

The quantification of adhesion through the segmentation and analysis of live-cell imaging data also supports the characterization of adhesion at the single-cell level. Specifically, cells in consecutive images were matched through a Bayesian cell tracking algorithm (btrack), relying on a probabilistic model of cell movement, spatial information, and cell appearance.[17]

Pairing this information with the corresponding adhesion status led to the identification of nine different adhesion dynamics (Table I). These vary greatly in terms of length, complexity, and prevalence within the population. Figure 2 reports relevant examples of such tracks (panels a–d) and their relative prevalence [Fig. 2(e)]. Each track in Figs. 2(a)–2(d) shows the behavior of one cell. For both cell lines, short tracks like the ones shown in Fig. 2(a) were the most common (86% and 89% for PEO1 and PEO4, respectively). The main reason for their prevalence is that they combine several different situations,

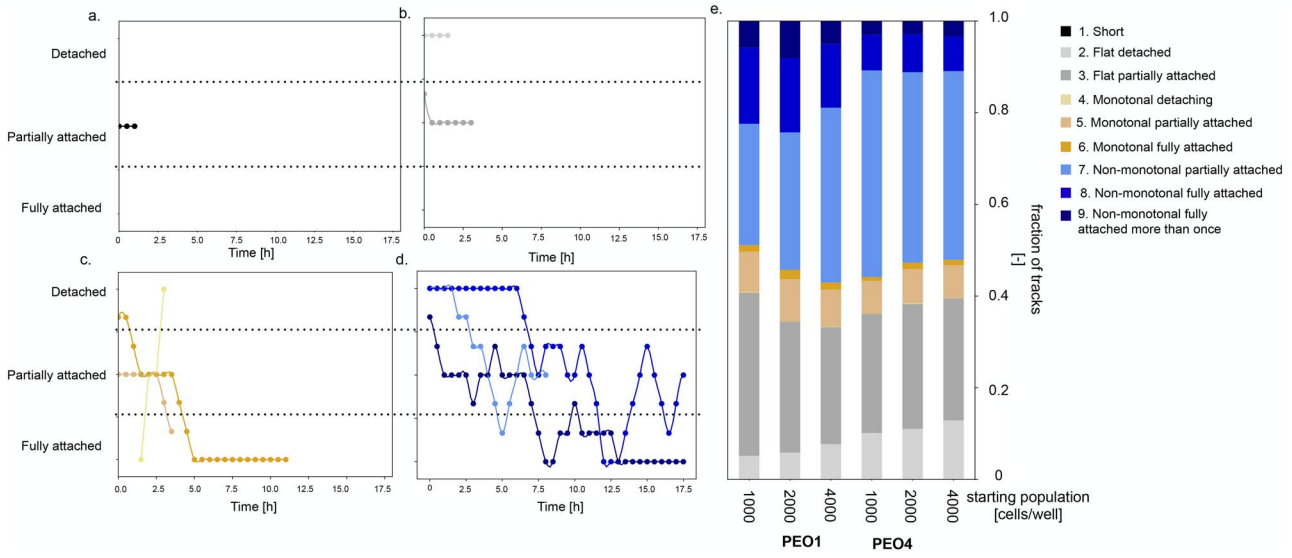


**FIG. 2.** Analysis of the adhesion dynamics of individual cells. (a) Representative example of a short track, i.e., a track shorter than 2 h. (b) Representative examples of flat tracks. These are longer than short tracks, defined by a small dynamic range and can be either detached or partially attached. (c) Monotonal tracks maintain the same direction of change, either upward (detaching) or downward (attaching). The latter has been divided between attaining full attachment (monotonal fully attached) or remaining at the partially attached stage (monotonal partially attached). (d) Non-monotonal adhesion tracks can also attach completely (non-monotonal fully attached) or stop at the partially attached stage (non-monotonal partially attached). In some cases, full attachment was observed multiple times for the same cell (non-monotonal fully attached more than once). (e) Prevalence of each track type for each considered condition (PEO1 and PEO4 cells, 1000, 2000, and 4000 cells/well). Short tracks were excluded in making of this plot, and each dot in panels (a)–(d) represents a measure.

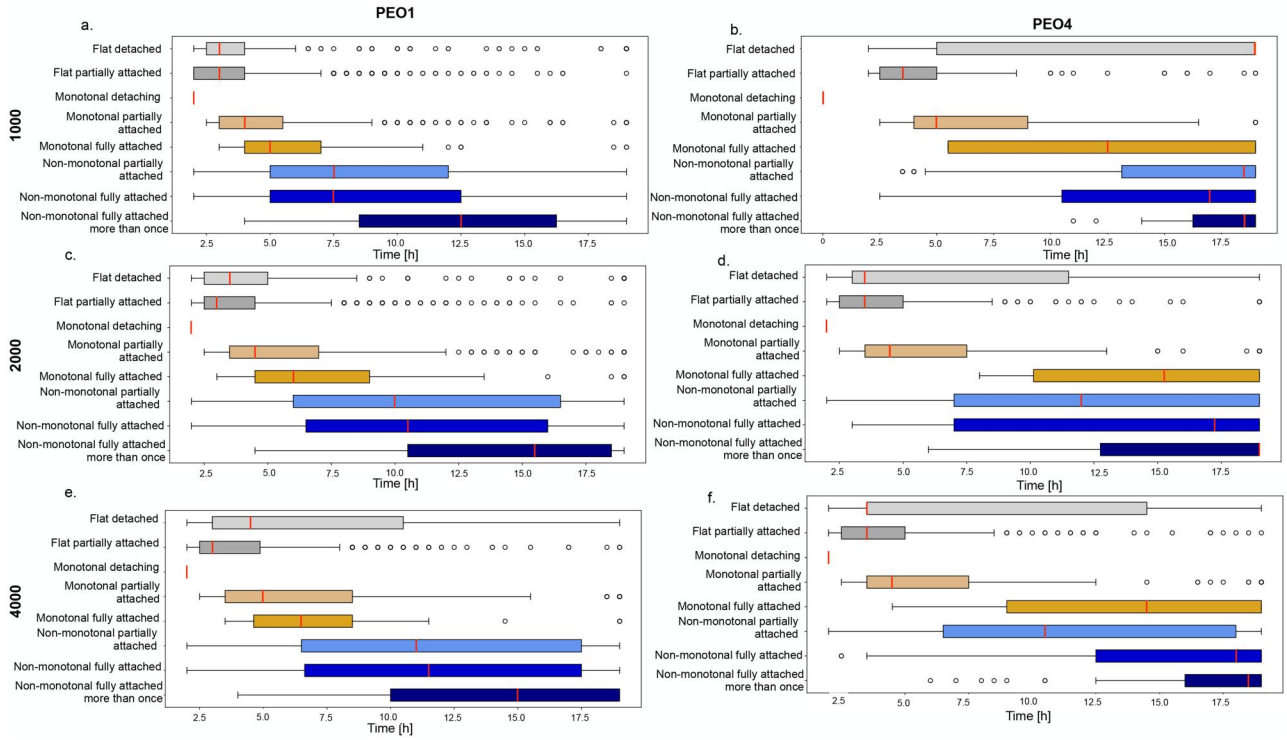


**FIG. 3.** Study of the distribution of track length. Each panel reports the result for each cell line and initial cell density. The boxplots describe the distribution of track length for each adhesion dynamic (identified by the labels on the y-axis and the colors). Orange bars mark the median of the distributions, while the edges of the colored boxes are the interquartile range. Short tracks (tracks with length less than 2 h) were excluded.

including cells that were not alive at the time of seeding, cells that exited the field of view during tracking, and newly divided cells at the end of the experiment. They were excluded from most of the analysis that follows as they would have required the use of separate methods, due to their short length and their adhesion status was mostly constant throughout the experiment.

Flat, partially attached tracks [representative examples shown in Fig. 2(b)] were also common [Fig. 2(e), supplementary material Table 1], together with the non-monotonal behavior, leading to a partial attachment of the cell [light blue in Figs. 2(d) and 2(e) and supplementary material Table 1]. Monotonal tracks [representative examples in Fig. 2(c)] were overall the least likely [Fig. 2(e), supplementary material Table 1]. Attainment of full attachment was the most common for PEO1 cells (on average, 23% of the non-short tracks vs 12% for PEO4 cells). A statistical analysis of the prevalence of each adhesion dynamic has been conducted to show how the median likelihood of each track type changes with cell line and seeding density (supplementary material Fig. 1). Differences between cell lines are the most common, even though variation among seeding densities was also observed [e.g., flat partially attached tracks for PEO1 cells; see supplementary material Fig. 1(b)].

## C. The length of the adhesion track is proportional to its complexity

An analysis of the track length (Fig. 3) revealed some notable differences both between adhesion dynamics and cell lines. Track complexity (e.g., non-monotonicity and attainment of full adhesion) was directly correlated with track length, with the "non-monotonal fully attached, more than once" behavior associated with a median length of at least 12.5 h [Fig. 3(a)]. A high variability in track length was, however, recovered for most track types (Fig. 3). This was particularly evident for PEO4 cells, where the interquartile range spanned more than 10 h for most conditions [Figs. 3(b), 3(d), and 3(f)].

## D. Cell doubling occurs early, and its probability depends on the cell's adhesion dynamic

One of the main features of btrack is the lineage tree reconstruction, which enabled the identification of cell doubling and kept track of each cell's parent and offspring. Despite the average doubling time for both PEO1 and PEO4 cells being longer than the duration of our experiment (at least 36 h[15]) we detected several cell divisions during our experiments.

Figure 4(a) shows the growth ratio, defined as the ratio between final and initial number of cells. PEO1s have a median growth ratio of about 1, corresponding to the maintenance of a stable population. A non-negligible variability among the replicates was, however, observed, together with a trend toward lower growth when a higher cell density was considered. This dependence of the proliferation rate on the population size was further confirmed by the percentage of cells that were observed dividing during the experiment [Fig. 4(b)]. Indeed, the number of proliferating PEO1 cells more than doubled

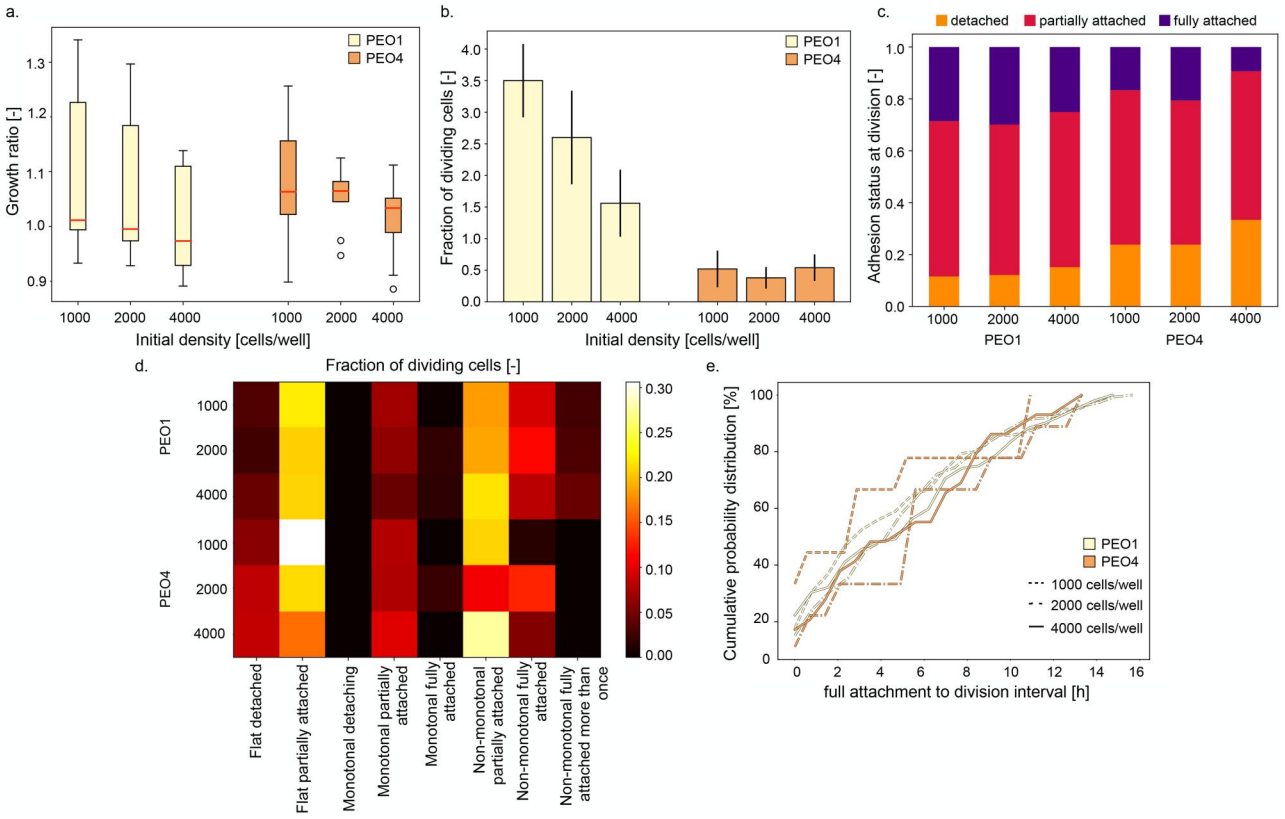


**FIG. 4.** Analysis of cell doubling (conducted excluding short tracks). (a) Distribution of growth ratios as a function of cell line and initial cell density. (b) Fraction of cells for which division was recorded organized by cell line and initial density. (c) Prevalence of each adhesion status (orange—detached, red—partially attached, and purple—fully attached) recorded at cell division. (d) Fraction of dividing cells by adhesion dynamic. (e) Cumulative distribution of the time interval between attainment of full attachment and cell division. The cumulative distribution represents the likelihood of the variable on the x axis to be less than or equal to the reported values.

when the initial population density was lowered from 4000 to 1000 cells/well.

PEO4 cells, on the other hand, showed a slightly higher median growth ratio (about 1.1) and a reduced dependency on the initial population size [Figs. 4(a) and 4(b)]. Another important difference was the reduction in the fraction of proliferating cells observed for this cell line, which dropped by about an order of magnitude [Fig. 4(b)].

Division was most likely to occur when cells were partially attached [Fig. 4(c)]. Figure 4(d) reports the breakdown of the fraction of dividing cells by adhesion dynamic. Interestingly, full attachment was not required for doubling to occur. Indeed, for both PEO1s and PEO4s, most of the cells that were observed dividing were classified as "flat partially attached" and "non-monotonal partially attached." Full attachment was generally associated with low probability of division, especially following a monotonal track. When cells attaining full attachment divided, they were likely to do it soon after complete adhesion [Fig. 4(e)]. Indeed, the cumulative distribution of the interval between full attachment to the substrate and cell division reached 50% between 4 and 6 h for all conditions.

We then focused our attention on the daughter cells, that is, the cells that were recorded by btrack to have a parent ID different from their own. Figure 5 shows the distributions of track start times for

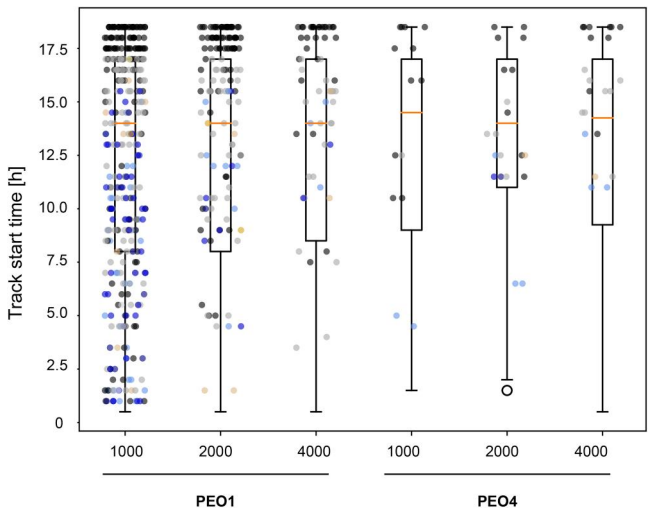


**FIG. 5.** Start time distributions for the daughter cells, that is, cells that were not present when the experiment started. Each dot represents a cell and is color-coded according to the corresponding adhesion dynamic.

these cells, separated by cell line and initial population density. Each dot represents a cell, color-coded according to its adhesion dynamic. This plot clearly shows the difference in number of division events recorded for each condition, even though the median start time was about 10 h in all cases. More complex tracks are generally associated with an earlier start time, but full adhesion was still observed in cells whose tracking started less than 5 h from the end of the experiment.

### E. Substituting the segmentation algorithm does not affect the results of the adhesion analysis

As highly specialized instruments such as the IncuCyte S3 Live Cell Analysis system are unlikely to be widely available, we decided to repeat the same analysis with a custom-made segmentation software.[18] This would extend the applicability of our method to other live-cell monitoring systems and images acquired with standard microscopy setups. This analysis was undertaken only for two initial cell densities (2000 and 4000 cells/well).

Figure 6 shows the comparison between the results obtained with the algorithm in Ref. 18 and the ones presented in Secs. II A and II B. In Fig. 6(a), the Jaccard index [Eq. (1)] of the two segmentations is shown. This is a similarity metric that evaluates the fraction of shared foreground pixels between two segmented images (A and B) by dividing their intersection or the area of overlap ($|A \cap B|$) by the total foreground area (e.g., their union, $|A \cup B|$):

$$J(A,B) = \frac{|A \cap B|}{|A \cup B|}. \quad (1)$$

A comparable distribution of Jaccard indices was observed for all tested conditions [Fig. 6(a)], confirming that cell shape and density did not affect the quality of the segmentation. The analysis of the global adhesion dynamics was also equivalent [Figs. 6(b) and 6(c), and supplementary material Fig. 2]. This was demonstrated through the Bland–Altman plot, which compares the difference between the results of two methods to their average. As most points (99.9% and 97.4% for PEO1 and PEO4, respectively) are within the 95% confidence interval [Figs. 6(b) and 6(c)], the global adhesion analysis obtained with custom segmentation can be considered equivalent to the one shown in Fig. 1.[19,20] This is also supported by the global adhesion dynamics obtained with the custom segmentation (supplementary material Fig. 2). Comparing these graphs to the ones in Fig. 1, the same trends and overall behavior are observed. The main difference was the initial prevalence of partially attached PEO4. Indeed, they are about as numerous as the detached ones in supplementary material Fig. 2, while in Fig. 1, they are about half as likely. This was probably connected with the classification procedure and the thresholds used to distinguish the different adhesion states. These values were empirically chosen for the segmentations obtained with the IncuCyte proprietary software but were also applied when the custom algorithm was used. This choice simplifies the comparison between the two methods and was justified by the high similarity between the two

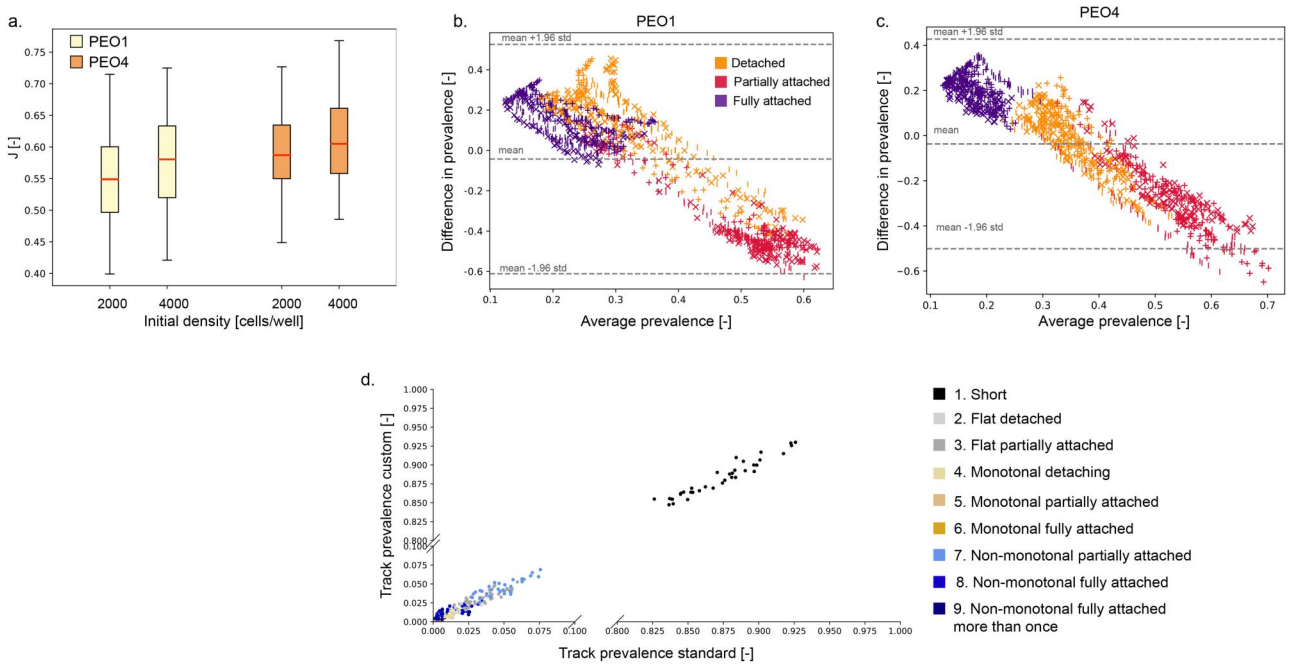


**FIG. 6.** Comparison between the results obtained with the two segmentation methods. (a) Jaccard index [Eq. (1)] quantifying the superimposition between the two segmentations of the same image. (b) The Bland–Altman plot comparing the two segmentation algorithms for PEO1 cells. Each point represents the prevalence of one adhesion class at a specific timepoint (initial cell densities and replicates have been kept separate). Different colors identify the corresponding adhesion stages (orange: detached, red: partially attached, and purple fully attached), while markers were used to separate the initial cell densities (x: 2000 cells/well, |: 4000 cells/well). (c) Same as (b) but for PEO4 cells. (d) Correlation between the prevalence of each track type as measured by the standard segmentation algorithm (x axis) or the custom approach (y axis). Colors identify the different track types.

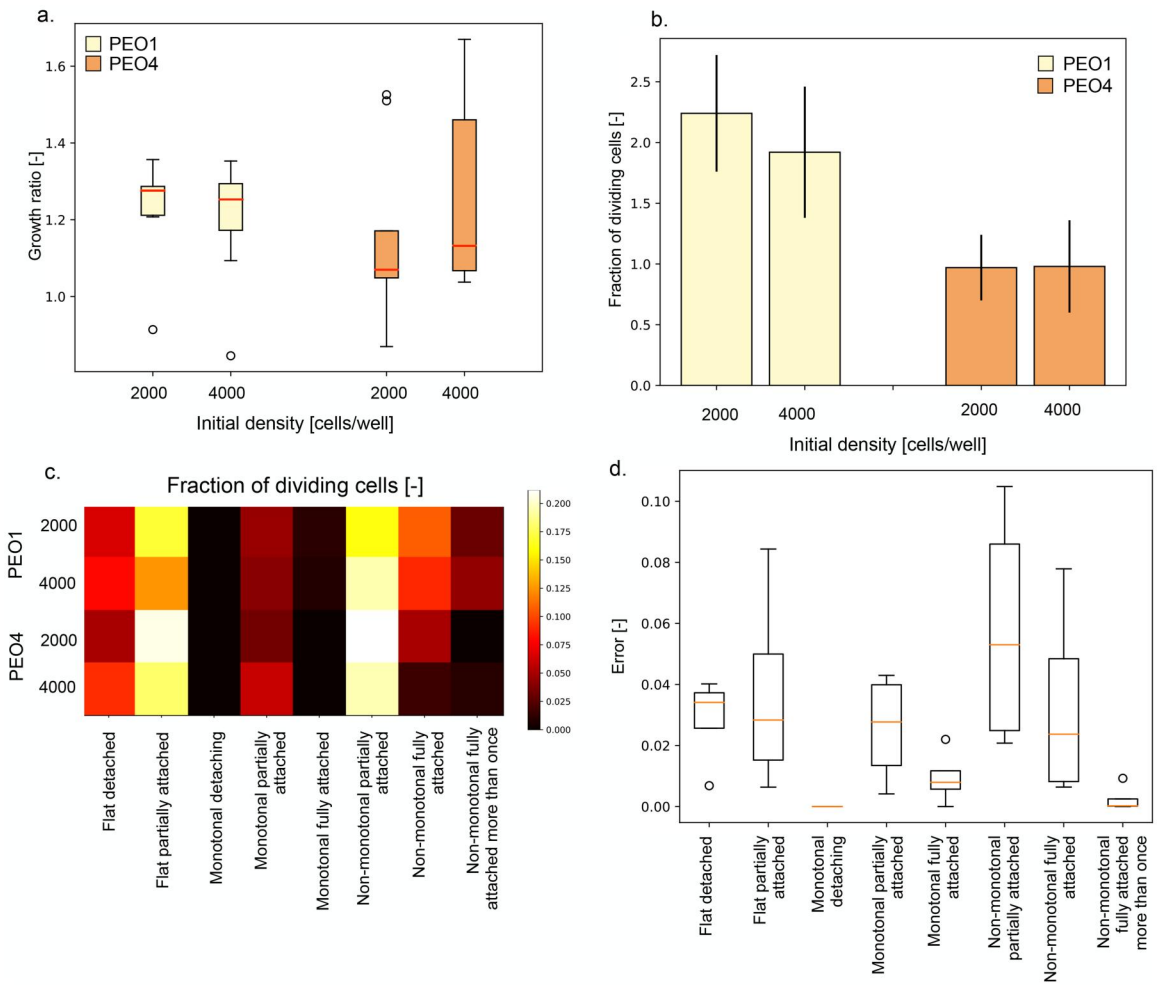


**FIG. 7.** Analysis of cell doubling using the custom segmentation algorithm. (a) Growth ratio distribution measured for each cell line and starting condition. (b) Average (±standard deviation) of the fraction of dividing cells. Each bar comprises data from three wells (three image stacks/well). (c) Heatmap showing the fraction of dividing cells organized by track type. (d) Error between the fraction of dividing cells in Figs. 5(c) and 8(c).

segmentations [Fig. 6(a)] but might lead to a slightly sub-optimal classification of the adhesion stages for the custom algorithm.

The prevalence of the different adhesion dynamics was also highly correlated [$R^2 = 0.999$, Fig. 6(d), supplementary material Fig. 3]. This result confirms that the equivalence of the two segmentation methods extends to the single-cell level analysis. Indeed, very similar tracking results were obtained, both in terms of track type prevalence [supplementary material Fig. 3 and Fig. 2(d)] and track length (supplementary material Fig. 4 and Fig. 3).

### F. The use of a custom segmentation algorithm does not affect the analysis of early cell doubling

Figure 7(a) shows the growth rate distribution obtained with the custom algorithm. When compared with Fig. 4(a), the median population growth was slightly higher (about 1.2 for all conditions), and the effect of initial cell density was less noticeable. The fraction of doubling cells, however, was highly consistent between the two methods [Figs. 7(b) and 4(b)]. PEO1 cells were associated with a higher fraction of dividing cells, and there was a trend toward reduced proliferation when a higher initial cell density is considered. PEO4 cells, on the other hand, maintained a similar fraction of doubling cells independently of the initial population. Breaking down the fraction of dividing cells according to their adhesion dynamic also yielded similar results. In addition to comparing Fig. 7(c) to Fig. 4(c), we also calculated the error distribution for each track type [Fig. 7(d)]. While the distribution variability changed between the different adhesion dynamics, the error was below 10% in all cases.

The start time distribution for the daughter cells was also largely conserved between the two segmentation algorithms (Figs. 8 and 5). The median start time was just under 13 h, and there was a direct correlation between track complexity and start time. While there was some variation in the number and distribution of recorded division events (color-coded dots in Figs. 8 and 5), the same conclusions can be derived from both figures.

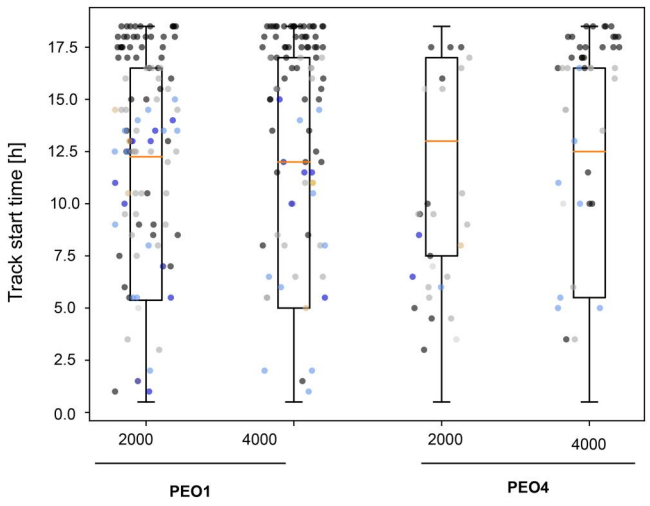


**FIG. 8.** Analysis of the distribution of start times according to the cell line and initial cell density. Each dot represents a daughter cell, and the color identifies the corresponding track type.

## III. DISCUSSION

We have presented an analysis pipeline for the quantification of cell adhesion from microscopy images. This novel method provides several advantages with respect to the currently available procedures, being characterized by high temporal resolution and by the possibility of distinguishing three different adhesion levels (detached, partially attached, and fully attached). The segmentation of individual cells, additionally, enables the study of their individual adhesion dynamic, a unique feature of this approach that yielded interesting insights into the adhesion process, and how it varies between cell lines. The pipeline that we have described is high throughput, largely automated, and its results are operator independent. These features, together with the possibility of changing the instrument used to acquire the images and the segmentation algorithm, suggest that this method could become the new standard for the evaluation of cell adhesion *in vitro*.

Indeed, the population level results that we obtained are largely equivalent to those of more traditional approaches[16] that show PEO1 cells adhering more quickly than PEO4s. While a more extensive analysis of this difference is needed, it might indicate a change in adhesion with OC progression. Earlier stages of the disease, represented by PEO1 cells, might be able to adhere more effectively as this feature would promote cancer dissemination and progression. A more advanced disease (PEO4 cells), on the other hand, might be less dependent on its ability to attach to a healthy tissue, thus divert resources toward the development of treatment resistance and improved cell survival. This hypothesis is further supported by the increased variability that we observed for PEO4 cells. Indeed, a more heterogenous population has been associated with increased robustness and improved survival in changing environments.[21] Traditional population level measurements, however, are unable to quantify this property as they focus on the difference between populations, rather than among individual cells.

Another result presented in this work is the limited effect that changing the initial cell density has on adhesion. This suggests that, in the tested conditions, space availability on the surface of the plate was not a limiting factor. While unexpected, given the fourfold change in the population size that we considered, these data demonstrate the robustness and accuracy of our approach across a wide range of population sizes, thus further increasing its potential scope of application.

The feature that sets the proposed method apart from the available alternatives, however, is the possibility of analyzing adhesion dynamics at the single-cell level. Nine different adhesion dynamics, varying both in length and complexity of the adhesion track, were identified. While the prevalence of each track type was largely conserved across the different tested conditions, full attachment was more common for PEO1 cells, in agreement with the population level results. Track length tended to be proportional to complexity, with cells attaining full adhesion, or following a non-monotonal path generally characterized by longer tracks. A non-negligible variability was, however, observed. This was particularly obvious for PEO4 cells, which tended to be characterized by longer tracks and a reduced difference between the length of tracks with different dynamics.

Another feature of the tracking algorithm used in this work is its ability to reconstruct the lineage tree for each tracked cell. This enabled us to identify several cell division events and connect them to specific adhesion dynamics. Indeed, despite having a reported doubling time of 37 and 36–46 h, respectively,[15] both PEO1 and PEO4 cells underwent division as early as 1 h after the beginning of the experiment (Figs. 4 and 7). This proliferation was not associated with a significant growth ratio [Figs. 4(a) and 7(a)], but the fraction of dividing cells was higher for PEO1 and inversely correlated with the initial cell density [Fig. 4(b)]. This phenomenon is coherent with a partial preservation of contact inhibition of proliferation in PEO1 cells. Indeed, while this is a mechanism mostly assumed to be disrupted in malignant cells, recent publications suggest that some cancer cells might still maintain sensitivity to contact inhibition.[22] The loss of proliferation inhibition with a larger initial cell population observed for PEO4 cells could be an indication of further disruption of the mechanisms that help maintain a stable cell population as the disease progresses.

An analysis of the adhesion dynamics most likely to be associated with division events [Figs. 4(d) and 7(c)] highlighted that how full attachment is not required for cells to double, and that a more looser dynamic attachment might favor early division. Indeed, while disassembly of adhesion complexes and cell rounding has been consistently observed before division to make space for the mitotic spindle and facilitate its alignment,[23,24] full attachment to the substrate has generally been considered as the starting point for this process. The results presented in this work [Fig. 4(c)] paint a more complex picture, with adhesion and proliferation occurring simultaneously and at different rates in different cell sub-populations. A partial confirmation of this observation is presented in Ref. 25, where cells seeded on a low adhesion surface exhibited a reduced expression of focal adhesion proteins and a more unstable attachment to the substrate. These characteristics resulted in higher rates of proliferation and migration, similarly to our results. While the comparison with Ref. 25 is limited by differences in experimental models and assays, the connection between a fluid, dynamic attachment, and a more aggressive cell phenotype can be established. This is particularly relevant for non-monotonal tracks, whose observed behavior could be connected with a higher metastatic potential and the cells' ability to better adapt to the environment.

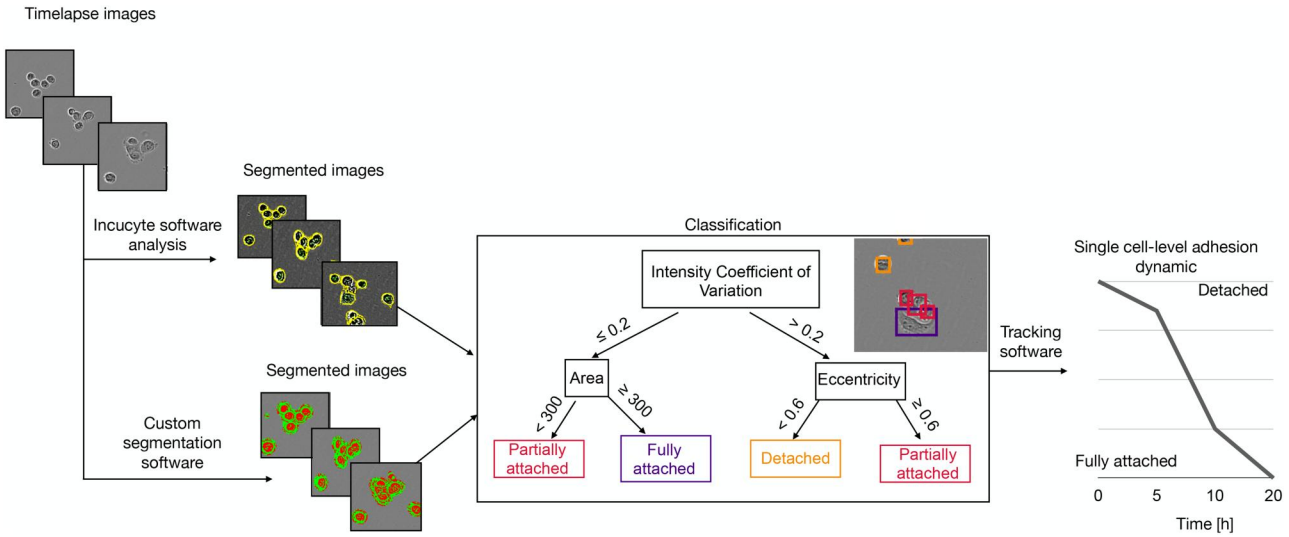


**FIG. 9.** Flowchart providing an overview of the analysis. Timelapse images of PEO1 and PEO4 cells during the adhesion process were segmented using IncuCyte S3 Live Cell Analysis System proprietary software. The segmented cells were classified according to their adhesion status using morphological and grayscale intensity features. A tracking algorithm was then applied to match individual cells across consecutive images and retrieve their individual adhesion dynamic. The same analysis was then repeated with a custom-made segmentation software[18] to test the dependency of the results on the segmentation software.

Overall, these results underscore the need for the development and use of experimental techniques able to capture the complexity and variability of biological processes.

## IV. CONCLUSION

In this work, we have presented a novel approach for the quantification of cell adhesion *in vitro*. This method addresses the major limitations of the standard approach for the evaluation of adhesion (low throughput, laborious procedure, and lack of standardization) while yielding more complete information. Indeed, it enables a notable increase in the temporal resolution of the analysis while providing a breakdown of three different adhesion stages and enabling the study of adhesion at the single-cell level. The independence of the results from the segmentation algorithm, demonstrated by repeating the analysis using two different methods, greatly expands the potential and scope of the proposed approach, making it independent of the live-cell monitoring instrument available and potentially applicable to standard microscopy setups.

While it was developed and tested exclusively on OC cells, this method is likely to be largely applicable to many different eukaryotic cultures. Indeed, detached and partially attached cells tend to be characterized by a fairly round and regular shape irrespective of their morphology when adhered.[26] Any modification to the segmentation algorithm or adhesion classification routine that might be necessary to improve performance in specific cell types can be easily implemented and integrated in the presented workflow, due to its modular structure.

Finally, the results obtained with this method shed new light on the complexity and variability of cell adhesion and could be the basis for further investigations into the role of doubling time and other cell- and environment-specific factors in this process.

## V. METHODS

### A. Overview of the analysis pipeline

Figure 9 provides an overview of the method. Images of live OC cells at the bottom of the plate were segmented to retrieve the outline of each cell. Two different algorithms were used at this stage to test the dependency of the results on the proprietary software of the IncuCyte S3 Live Cell Analysis system.

Specific morphological and intensity features were used to classify each cell according to its adhesion status (detached, partially attached, or fully attached). This enabled the study of the prevalence of each adhesion class, and how it changed over time. This analysis was repeated by changing the initial cell seeding density, to determine if space availability on the plate surface would influence cell adhesion.

The btrack tracking software[17] was then used to match individual cells across consecutive images and retrieve their specific adhesion dynamic. This increase in resolution is one of the main features of this analysis pipeline and provided novel insights into cell adhesion.

### B. Cell culturing and adhesion experiments

OC cell lines PEO1 and PEO4 were kindly donated by Professor Deborah Marsh (University of Technology Sydney, NSW). They were maintained in the Roswell Park Memorial Institute (RPMI) medium (Thermo Fisher, USA) supplemented with 10% fetal bovine serum-FBS (Sigma-Aldrich, USA), 1% Pen-Strep (Sigma-Aldrich, USA), and 1% GlutaMAX (Thermo Fisher, USA) in standard cell culture conditions (37 °C and 5% $CO_2$). For the adhesion experiment, three different seeding densities (1000, 2000, or 4000 cells/well) were used for each cell line. Cells were detached by incubation with Trypsin-EDTA (0.5%) (Thermo Fisher, USA) for up to 2 min. Complete medium was used to stop the detachment and wash the cells prior to seeding in a 96-well plate (i.e., Nunclon Delta-treated, Flat-Bottom, 6 wells/condition, 100 $\mu$l/well). Immediately after seeding, the plate was transferred to the

IncuCyte S3 Live Cell Analysis System (Sartorius, Germany). Three non-overlapping images (1408 × 1040 px) for each well were acquired with a magnification of 10× every 30 min for a total of 20 h. The acquisition of multiple images/well improves sampling, by increasing the percentage area of the plate that is monitored during the experiment. The total duration of the experiment was set to 20 h, with images acquired every 30 min. These parameters are coherent with the time scales of cell adhesion and doubling,[15,16] the main processes involved in this experiment.

### C. IncuCyte software segmentation and adhesion status determination

The IncuCyte proprietary analysis software was used to analyze the images and retrieve the cells' outlines. All the segmentation parameters were left at their default value. Images were then exported in the tif format. The segmentation was completed by filling holes with area <2000 px. Objects comprising 50 px or less were considered to be debris and disregarded. A custom-made Python (v 3.9) script was used to determine the adhesion status of each segmented cell (Fig. 9). It relies on three parameters that characterize the morphology and brightness of cells. Eccentricity [E, Eq. (2)] is a measure of roundness calculated as the ratio between the focal distance (FD) and the length of the major axis (M) of the ellipse that best approximates the cell. This index varies between 0, for perfectly spherical objects, and 1 for highly elongated ones:

$$E = \frac{FD}{M}. \tag{2}$$

The coefficient of variation of the intensity [CV, Eq. (3)] is the ratio between the standard deviation and the mean of the values of all the pixels classified as part of the cell. It can be used as a metric of contrast, as cells featuring a wide range of intensity values will have higher CV than ones with more homogeneous gray levels,

$$CV = \frac{\sigma}{\mu}. \tag{3}$$

Finally, the area of the cell (A) is a quantification of the space it occupies. For this analysis, we define area as the number of pixels belonging to each cell as it maintains accuracy irrespective of cell shape and its regularity. Detached cells are round and have high contrast, as such cells with an $E < 0.6$ and $CV > 0.2$ were classified as detached. Conversely, fully attached cells were identified by their larger area ($A \geq 300$ px) and lower contrast ($CV \leq 0.2$). All the other cells were assigned to the intermediate partially attached group (Fig. 4). These thresholds were determined empirically for the images used in this analysis and might require adjustments when using a different experimental model. A sensitivity analysis was, however, conducted to determine the effect of changing the adhesion classification thresholds. In all cases, four equispaced values between −10% and +10% of the reference value were chosen (Table II). For each possible combination of these parameters, the adhesion status classification was determined. Each adhesion status was assigned a number (detached → 1, partially attached → 2, and fully attached → 3), and the percentage difference between the adhesion status corresponding to each parameter set and the reference value was calculated. This resulted in an error between 0 (the cell maintains its classification) and 2 (a fully attached cell becomes detached or vice versa).

**TABLE II.** Parameter values used for the sensitivity analysis.

| Parameter | Values | Reference value |
|---|---|---|
| $E_s$ | 0.54, 0.57, 0.63, 0.66 | 0.6 |
| $CV_s$ | 0.18, 0.19, 0.21, 0.22 | 0.2 |
| $A_s$ (px) | 270, 285, 315, 330 | 300 |

Figure 10 shows the results of this analysis where errors have been grouped according to the distance between the two parameter configurations [Eq. (4)]. The classification error remained below 15 % for all tested configurations, with a median error of less than 10 % in all cases. This low sensitivity to changes in the parameters highlights the stability of our method and its suitability for the analysis here described,

$$Distance = \frac{|CV_s - CV_{ref}|}{CV_{ref}} + \frac{|A_s - A_{ref}|}{A_{ref}} + \frac{|E_s - E_{ref}|}{E_{ref}}. \tag{4}$$

### D. Custom-made segmentation algorithm

The custom-made segmentation algorithm used in this work was initially described in Ref. 18. It was programmed with MATLAB 2021b Image Processing Toolbox™. Cells on phase contrast image stacks were divided into sections based on relative pixel intensity compared to image background.

For the analysis here presented, only the dark areas (green channel) were used, and, as with the previous algorithm, objects with area <50 px were disregarded. No modification to the adhesion classification routine or the tracking software was implemented.

The similarity of the two segmentations was evaluated through the Jaccard index [Eq. (1)]. This metric was computed independently for each image and then grouped according to the experimental condition (cell line and initial cell density).

### E. Global adhesion analysis

Population-level adhesion was quantified by computing, for each time point and experimental condition, average and standard deviation of the prevalence of each adhesion status. The number of cells in the first image of each series was used as normalizer.

The Bland–Altman plot was used to compare the results of the global analyses obtained with the two segmentations. This graph plots the difference between the results of the two methods as a function of their average. Horizontal lines identify the average and 95% confidence interval of the difference.

### F. Tracking software

The Bayesian tracking software btrack[17] was used to match individual cells across images and retrieve their adhesion dynamic. It relies on a Bayesian belief matrix and a cell motion model to construct tracklets that describe the position of each cell up until cell division. Multiple hypothesis testing is then performed to assemble the tracklets into tracks and retrieve each cell's lineage tree.[17] The default parameters were used during the optimization procedure due to the similarities between the experimental setup in Ulicna *et al.*[17] and

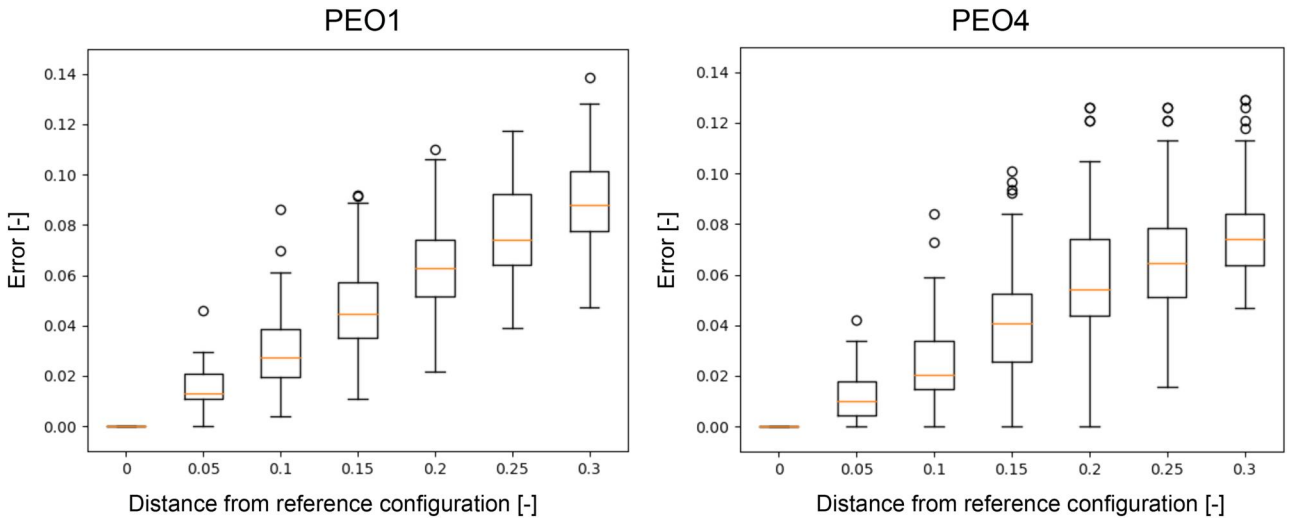


**FIG. 10.** Sensitivity analysis showing the effect of changing the adhesion classification parameters on the results. The distance from the reference configuration was calculated as in 4, while the error was proportional to the change in adhesion status between the two configurations. No change was associated with an error of 0, while reclassification from fully attached to detached (and vice versa) was associated an error of 2.

the one used in this work. For some of the image stacks (Table III), the optimization failed. This was likely caused by a combination of imprecisions in the cell movement model, which was initially developed for a non-cancerous epithelial cell line[17] and low temporal resolution of the experiment. Indeed, cell division was unexpectedly shown to occur early and frequently. This reduced the overall length of the tracklets and potentially led to optimization failure. Future developments of this work will address these limitations.

Image stacks for which the optimization failed were excluded from this analysis. As no data were available for the condition PEO1 cells, 1000 cells/well using the custom segmentation method, we decided to exclude this cell density from the analysis relying on this approach.

## G. Single-cell level adhesion analysis

The tracks were analyzed to determine how each cell's adhesion status changed throughout the experiment. The classification procedure described in Sec. V C (Fig. 9) was applied, and the resulting adhesion tracks were smoothed by applying a moving average with a window size equal to 3. This procedure was used to avoid rapid short switches in the adhesion status, which would be likely caused by the cell's properties being close to the classification thresholds. This step was not applied to tracks shorter than 4 h as per the definition of moving average.

**TABLE III.** Summary of the failed btrack optimizations by experimental condition and the segmentation method.

| Cell line | Seeding density (cells/well) | Incucyte segmentation | Custom segmentation |
|---|---|---|---|
| PEO1 | 1000 | 5/9 | 9/9 |
| PEO1 | 2000 | 1/9 | 4/9 |
| PEO1 | 4000 | 0/9 | 0/9 |
| PEO4 | 1000 | 0/9 | 0/9 |
| PEO4 | 2000 | 0/9 | 0/9 |
| PEO4 | 4000 | 0/9 | 0/9 |

This analysis identified nine different adhesion dynamics (Table I). Individual tracks were sorted automatically according to the following procedure. Short tracks were identified by their length (<2 h). The range of the variation then was calculated. If it was less than 1/6 of the available dynamic range, the track was classified as flat. The distinction between flat, detached, and partially attached was made according to the corresponding adhesion status. The remaining tracks were then divided between monotone and non-monotone. For monotone tracks, the last recorded adhesion status was compared to the first one. This enabled the distinction between detaching and attaching cells. The last adhesion status was also used to distinguish between monotonal partially attached and monotonal fully attached. A similar approach was used to identify non-monotonal partially attached tracks. All the remaining dynamics were non-monotonal with full attachment. The number of adhesion events was evaluated as the number of continuous stretches of the track classified as being fully attached [2 in Fig. 2(d)].

The prevalence of each adhesion dynamic was determined as the average fraction of tracks in each class following the exclusion of the short tracks. This was necessary due to the high prevalence of short tracks with late start time (Fig. 5), which would have overshadowed the dynamics observed at earlier timepoints.

## H. Analysis of the doubling events

The optimization step in btrack enables the reconstruction of the lineage trees, thus the identification of division events and of the cells involved in this process. In our analysis, we focused both on the dividing cells and on the new cells that were generated during the experiment. For the former, we determined their prevalence within the

population (number of cells determined to have undergone division divided by the total number of tracked cells) and the adhesion status immediately prior to cell doubling and adhesion dynamic. The adhesion dynamic was evaluated also for the newly born cells, together with the distribution of the start times for their track.

For the subset of cells attaining full adhesion, the cumulative distribution of the time interval between full attachment and division was also calculated. The absolute value of the difference between the fraction of dividing cells obtained with either the segmentation method was computed to provide an indication of the disparity of their results.

### I. Statistical analysis

Statistical analysis was conducted using the Kruskal–Wallis test, a non-parametric test, which compares the median of two populations to determine whether or not they are equal. A p value of 0.05 was considered as threshold for significance.

## SUPPLEMENTARY MATERIAL

See the supplementary material for the following: Table 1: Percentage prevalence of each adhesion dynamic organized by cell line and initial cell density. These values were calculated after the exclusion of short tracks. Statistical analysis for these data is provided in Fig. 1. **Supplementary Fig. 1:** Statistical analysis of the prevalence of each adhesion dynamic. The Kruskal–Wallis test was used to compare each condition and a p-value of 0.05 was chosen as threshold for significance. **Supplementary Fig. 2:** Global adhesion analysis for the custom segmentation algorithm. (a) Average and standard deviation of the fraction of cells in each adhesion status measured for PEO1 cells with an initial cell density of 2000 cells/well. (b) Same as (a) but with starting populations of 4000 cells/well. (c) and (d) The same analysis but for PEO4 cells. In all cases three wells/condition and three images/well were considered. **Supplementary Fig. 3:** Prevalence of each adhesion type retrieved with the custom segmentation algorithm. As in Fig. 2(e), short tracks were excluded. **Supplementary Fig. 4:** Study of the distribution of track length as a function of cell line, initial cell density, and adhesion dynamic. Segmentations obtained with the custom algorithm.

## ACKNOWLEDGMENTS

This project received funding from the European Union's Horizon 2020 research and innovation program under the Marie Sklodowska-Curie Actions (Grant Assessment No. 883172). The authors acknowledge the Katharina Gaus Light Microscopy Facility for the IncuCyte use.

## AUTHOR DECLARATIONS

### Conflict of Interest

The authors have no conflicts to disclose.

### Ethics Approval

N/A as only standard cell lines were used in this work.

### Author Contributions

**Marilisa Cortesi:** Conceptualization (equal); Formal analysis (lead); Funding acquisition (lead); Software (lead); Visualization (equal); Writing – original draft (lead). **Jingjing Li:** Formal analysis (equal); Methodology (equal); Software (equal); Writing – review & editing (equal). **Dongli Liu:** Conceptualization (equal); Data curation (equal); Investigation (equal); Writing – review & editing (equal). **Tianruo Guo:** Formal analysis (equal); Methodology (equal); Writing – review & editing (equal). **Socrates Dokos:** Conceptualization (equal); Supervision (equal); Writing – review & editing (equal). **Kristina Warton:** Conceptualization (equal); Supervision (equal); Writing – review & editing (equal). **Caroline E. Ford:** Conceptualization (equal); Funding acquisition (equal); Project administration (equal); Supervision (equal); Writing – review & editing (equal).

## DATA AVAILABILITY

The data that support the findings of this study are available from the corresponding author upon reasonable request.

## REFERENCES

[1]B. Alday-Parejo, K. Ghimire, O. Coquoz, G. W. Albisetti, L. Tamò, J. Zaric, J. Stalin, and C. Rüegg, "MAGI1 localizes to mature focal adhesion and modulates endothelial cell adhesion, migration and angiogenesis," Cell Adhes. Migr. **15**, 126–139 (2021).
[2]M. Cortesi, D. Liu, C. Yee, D. J. Marsh, and C. E. Ford, "A comparative analysis of 2D and 3D experimental data for the identification of the parameters of computational models," Sci. Rep. **13**, 15769 (2023).
[3]M. T. Guinn, Y. Wan, S. Levovitz, D. Yang, M. R. Rosner, and G. Balázsi, "Observation and control of gene expression noise: Barrier crossing analogies between drug resistance and metastasis," Front. Genet. **11**, 586726 (2020).
[4]A. Ahmad Khalili and M. R. Ahmad, "A review of cell adhesion studies for biomedical and biological applications," Int. J. Mol. Sci. **16**, 18149–18184 (2015).
[5]Q. Guo, L. Li, G. Gao, R. Liu, Y. Einaga, and J. Zhi, "Nanodiamonds inhibit cancer cell migration by strengthening cell adhesion: Implications for cancer treatment," ACS Appl. Mater. Interfaces **13**, 9620–9629 (2021).
[6]J. E. Murphy-Ullrich *et al.*, "The de-adhesive activity of matricellular proteins: Is intermediate cell adhesion an adaptive state?," J. Clin. Invest. **107**, 785–790 (2001).
[7]H. M. Eilken, S.-I. Nishikawa, and T. Schroeder, "Continuous single-cell imaging of blood generation from haemogenic endothelium," Nature **457**, 896–900 (2009).
[8]J. Li, O. Lao, F. F. Bruveris, L. Wang, K. Chaudry, Z. Yang, N. Farbehi, E. S. Ng, E. G. Stanley, R. P. Harvey *et al.*, "Mimicry of embryonic circulation enhances the HOXA hemogenic niche and human blood development," Cell Rep. **40**, 111339 (2022).
[9]T. Schroeder, "Imaging stem-cell-driven regeneration in mammals," Nature **453**, 345–351 (2008).
[10]M. V. Barbolina, "Molecular mechanisms regulating organ-specific metastases in epithelial ovarian carcinoma," Cancers **10**, 444 (2018).
[11]C. E. Ford, B. Werner, N. F. Hacker, and K. Warton, "The untapped potential of ascites in ovarian cancer research and treatment," Br. J. Cancer **123**, 9–16 (2020).
[12]R. Sheng, X. Li, Z. Wang, and X. Wang, "Circular RNAs and their emerging roles as diagnostic and prognostic biomarkers in ovarian cancer," Cancer Lett. **473**, 139–147 (2020).
[13]A. Kim, Y. Ueda, T. Naka, and T. Enomoto, "Therapeutic strategies in epithelial ovarian cancer," J. Exp. Clin. Cancer Res. **31**, 14 (2012).
[14]R. L. Siegel, K. D. Miller, N. S. Wagle, and A. Jemal, "Cancer statistics, 2023," CA Cancer J. Clin. **73**, 17 (2023).
[15]S. P. Langdon, S. S. Lawrie, F. G. Hay, M. M. Hawkes, A. McDonald, I. P. Hayward, D. J. Schol, J. Hilgers, R. C. Leonard, and J. F. Smyth, "Characterization and properties of nine human ovarian adenocarcinoma cell lines," Cancer Res. **48**, 6166–6172 (1988).
[16]S. J. Ritch, A. S. M. Noman, A. A. Goyeneche, and C. M. Telleria, "The metastatic capacity of high-grade serous ovarian cancer cells changes along disease progression: Inhibition by mifepristone," Cancer Cell Int. **22**, 397 (2022).

[17]K. Ulicna, G. Vallardi, G. Charras, and A. R. Lowe, "Automated deep lineage tree analysis using a Bayesian single cell tracking approach," Front. Comput. Sci. **3**, 734559 (2021).
[18]L. Wang, J. Li, B. R. Coad, C. D. McFarland, and R. E. Nordon, "Interaction of endothelial cells with plasma-polymer modified surfaces," Materialia **9**, 100613 (2020).
[19]N. Ö. Doğan, "Bland-Altman analysis: A paradigm to understand correlation and agreement," Turk. J. Emerg. Med. **18**, 139–141 (2018).
[20]J. Lovecchio, V. Betti, M. Cortesi, E. Ravagli, S. Severi, and E. Giordano, "Design of a custom-made device for real-time optical measurement of differential mineral concentrations in three-dimensional scaffolds for bone tissue engineering," R. Soc. Open Sci. **9**, 210791 (2022).
[21]R. Wollman, "Robustness, accuracy, and cell state heterogeneity in biological systems," Curr. Opin. Syst. Biol. **8**, 46–50 (2018).
[22]D. R. Grimes and A. G. Fletcher, "Close encounters of the cell kind: The impact of contact inhibition on tumour growth and cancer models," Bull. Math. Biol. **82**, 20 (2020).
[23]C. Luxenburg, H. Amalia Pasolli, S. E. Williams, and E. Fuchs, "Developmental roles for Srf, cortical cytoskeleton and cell shape in epidermal spindle orientation," Nat. Cell Biol. **13**, 203–214 (2011).
[24]R. Zaidel-Bar, "Cell cycle pacemaker keeps adhesion in step with division," J. Cell Biol. **217**, 2981 (2018).
[25]Y.-S. Park, Y. Choi, and J. S. Lee, "Focal adhesion dynamics-mediated cell migration and proliferation on silica bead arrays," Biomater. Sci. **13**, 1849–1857 (2025).
[26]A. Nyga, K. Plak, M. Kräter, M. Urbanska, K. Kim, J. Guck, and B. Baum, "Dynamics of cell rounding during detachment," Iscience **26**, 106696 (2023).